Assessment of regularization techniques used in electrocardiographic imaging

Matija Milanič[1], Vojko Jazbinšek[2], Rok Hren[2]

[1]*Jožef Stefan Institute, Ljubljana, Slovenia*
[2] *Institue of mathematics, Physics and Mechanics*
E-pošta: matija.milanic@ijs.si

Abstract

Electrocardiographic imaging (ECGI) is a widely used method of computing potentials on the epicardium from measured or simulated potentials on the torso surface. The main challenge of the electrocardiographic imaging problem remains its intrinsic ill-posedness, which requires use of regularization techniques to smooth out the solution; the amount of smoothing that is still clinically acceptable is a subject of ongoing research. In this study, we systematically compared various mathematical techniques in regularizing the ECGI problem. For the purposes of the forward computations, we employed potentials measured on the cylindrical cage placed around the physiological source (canine heart) and situated in the electrolytic torso tank. The inverse potentials on the cylindrical-cage surface were recovered using 14 different regularization techniques. We found that non-quadratic methods (total variation algorithms) were the most robust and resulted in the lowest reconstruction errors.

1 Introduction

In clinical practice, physician deduces from a limited number of electrocardiographic signals, highly complex electrical activity of the heart in terms of a simplified, i.e., equivalent, source model, which typically consists of a single rotating dipole. Such-to a large extent-qualitative approach to solving the electrocardiographic inverse problem still represents the cornerstone of a day-to-day diagnosis.

During the past 30 years, much research efforts have been devoted to exploring and validating the utility of electrocardiographic imaging, where equivalent potential distribution on the epicardial surface is inversely computed from the large number of electrocardiograms measured both on the anterior and posterior torso surface. It has been widely recognized that epicardial potentials directly reflect the underlying cardiac activity and could provide an effective means for localizing regional cardiac events. Electrocardiographic imaging problem, however, is inherently ill-posed in a sense that even small errors in measurements of potentials on the torso surface result in unbounded errors on the epicardial surface. This ill-posedness has been well studied in electrocardiography (e.g, [1-5]) and a plethora of regularization techniques have been applied to gauge rapidly oscillating inverse solutions. It seems that there is a growing need to better structure and unify various regularization methods and to that end, to compare individual approaches to regularization using the same volume conductor and the same cardiac source models.

In this paper, we have systematically evaluated the performance of 14 different regularization techniques using the physiological model of the heart; we have also compared boundary element method and finite element method, two methodologies which are in electrocardiography most often used to describe the geometrical and electrical properties of the volume conductor, confined by the irregularly-shaped epicardial and torso surfaces.

2 Methods

The equivalent potential distribution on the epicardial surface can be found from a known potential distribution on the torso surface by solving generalized Laplace's equation subjected to Cauchy boundary conditions [1-4]. Such a boundary-value problem must be in an arbitrarily shaped volume conductor approximated on a discretized solution domain as the system of linear equations. For the homogeneous and isotropic model of the human torso, this can be achieved by means of the boundary element method (BEM), which relates the potentials at the torso nodes (expressed as an m-dimensional vector Φ_B) to the potentials at the epicardial nodes (expressed as an n-dimensional vector Φ_E),

$$\Phi_B = \mathbf{A}\,\Phi_E \ , \qquad (1)$$

where $\mathbf{A}$ is the transfer coefficient matrix ($m \times n$) and $n < m$. The transfer coefficient matrix depends entirely on the geometric integrands which can be calculated analytically. Similar formalism as in (1) can be applied to the finite element method (FEM), with the difference that FEM discretizes the entire volume between the torso and epicardial surfaces into tetrahedral elements and can also take into account electrical anisotropies of the volume conductor.

The matrix $\mathbf{A}$ is ill-conditioned, i.e., its singular values are limiting to zero with no particular gap of

separation in the singular value spectrum, which yields an unstable solution. As mentioned above, the wild oscillations of the inverse solution need to be controlled by the regularization and the techniques we have used in our study are summarized in Table 1. For the sake of structuring, we subdivided regularization techniques into 3 groups: Tikhonov-based regularizations, iterative methods, and non-quadratic regularizations.

Table 1. Summary of 14 regularization techniques employed in our study. Techniques are subdivided into 3 main categories: Tikhonov-based regularizations (Group A), iterative methods (Group B), and non-quadratic methods (Group C).

Group	Acronym	Short description	Ref.
A	ZOT	Zero-order Tikhonov	[6,7]
	FOT	First-order Tikhonov	[4]
	SOT	Second-order Tikhonov	[7]
B	ZCG	Zero-order Conjugate Gradient	[8]
	FCG	First-order Conjugate Gradient	[8]
	SCG	Second-order Conjugate Gradient	[8]
	ZLSQR	Zero-order LSQR	[9]
	FLSQR	First-order LSQR	[9]
	SLSQR	Second-order LSQR	[9]
	TSVD	Truncated Singular Value Decomposition	[10]
	ν	ν-method	[10]
C	FTV	Total Variation	[4]
	STV	Total Variation with Laplacian	[4]
	LASSO	Least Absolute Selection and Shrinkage Operator	[11]

Our experimental protocol consisted of the following steps:

Step 1. For the purposes of modeling the cardiac source, we used an isolated heart preparation in which one canine heart was retrogradely perfused via the aorta by a second, support dog and suspended in the correct anatomical position in an electrolytic tank shaped like an adolescent thorax. We recorded electric potentials (at 1 kHz) from the 602-lead cylindrical cage enveloping the suspended canine heart and thus serving as the "epicardial" surface; geometries of torso and cylindrical cage surfaces are shown in Fig. 1. Data were collected during a sinus rhythm, with the sample epochs of 4-7 seconds in duration.

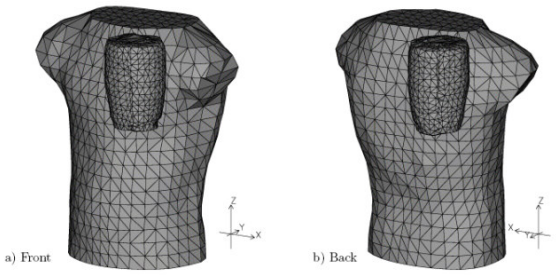

Figure 1.Geometries of the torso and cylindrical cage surfaces. Data recorded at 602 leads of the cylindrical cage were used to compute torso potentials at 771 nodes using BEM and FEM.

Step 2. The cylindrical cage potentials were then used to calculate torso potentials at 771 nodes using the BEM and FEM, respectively (Eq. 1); in both BEM and FEM, we assumed the volume conductor to be homogeneous and isotropic. Three measurement noise levels (20 dB, 40 dB, 60 dB) were added to the torso potentials to mimic experimental measurement conditions.

Step 3. The 602-lead cylindrical cage potentials were reconstructed by the 14 regularization techniques, summarized in Table 1, for each noise level and for BEM and FEM separately. [5] [1,3].

Step 4. We expressed the accuracy of the inverse solution in terms of the normalized rms (root-mean-square) error $RE = \| \Phi_E^c - \Phi_E^m \|_2 \ / \| \Phi_E^m \|_2$, and the correlation coefficient, $CC = \Phi_E^c \cdot \Phi_E^m \ / \|\Phi_E^c\|_2 \, \|\Phi_E^m\|_2$, calculated between measured and inversely computed cylindrical-cage potentials Φ_E^m and Φ_E^c, respectively. We also carefully examined qualitative features of measured and inversely computed maps (e.g., areas of negative potentials, positions of extrema).

3 Results

Table 2 illustrates reconstruction results during the initial phase of the QRS complex, from the Q-onset to the peak of the Q-wave, in the presence of a 40-dB noise and when using BEM. Even due to the low-signal-to-noise ratio right after the onset, cylindrical cage potentials were reconstructed with the rms normalized errors of 0,22-0,36 and correlation coefficients of 0,93-0,98, depending on the regularization technique used. It is evident that the most robust performance throughout the sequence was attained by the non-quadratic methods, either in the form of the total variation method (FTV) or the total variation algorithm with the Laplacian in the place of a gradient operator (STV).

Figure 2 depicts body surface potentials at 5 ms after the onset of the Q wave and corresponding measured and reconstructed cylindrical-cage potentials; potentials were recovered employing FTV and STV, in both cases along with BEM.As expected from the literature, body surface potentials exhibit initial anterior maximum, resulting from the left septal activation of the ventricles. Both FTV and STV capture well the qualitative features of the cylindrical-cage potentials, with STV providing smoother solutions.

Table 3 summarizes results for standard reference points of the sinus rhythm (peaks of P, R, S, and T waves), again in the presence of a 40-db noise and when using BEM. As in Table 2, both non-quadratic regularization techniques (FTV, STV) performed consistently better than other 12 methodologies tested. There were, however, time instants when there were little differences among various regularization techniques, and when some Tikhonov regularizations (FOT, SOT) and some iterative regularizations (FCG, SCG, FLSQR, SLSQR) were on a par with the non-quadratic techniques. Closer inspection of cylindrical cage potentials revealed that during those time instants, potential distributions were dipolar (i.e., exhibiting only a single maximum and minimum) and had rather simple

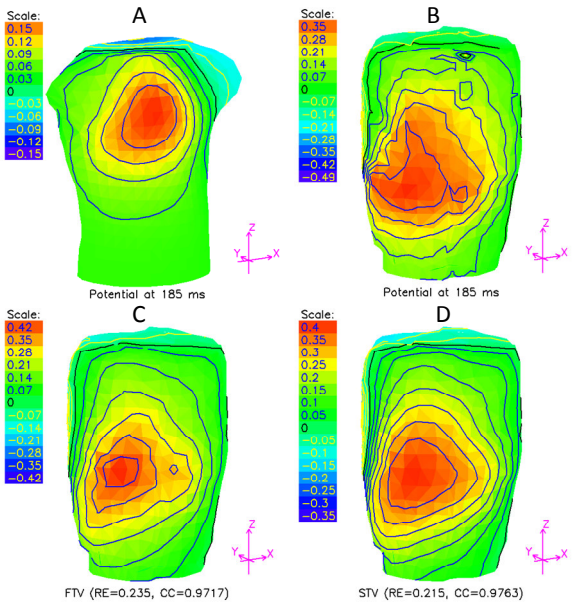

Figure 2. Potential distributions at 5 ms after the onset of the Q wave. (A) Torso potentials computed from the measured cylindrical cage potentials using boundary element method (BEM). (B) Measured cylindrical cage potentials. (C) Inversely computed cylindrical cage potentials using the totals variation method (FTV). (D) Inversely computed cylindrical cage potentials using the totals variation algorithm with the Laplacian instead of a gradient operator (STV)..

spatial features (e.g., well separated extrema). Even in such cases, results suggest that FTV and STV may become better than other techniques when the noise level is increased from 40 dB to 20 dB.

Comparison between BEM and FEM showed little difference, with BEM performing somewhat better than FEM. The difference between methodologies is due to lower condition number of matrix **A** for BEM than for FEM (by the factor of 73.1). As noted, this comparison

Table 2. Root-mean-square (rms) errors for reconstruction results during the initial phase of the QRS complex, from the Q-onset to the peak of the Q-wave, in the presence of a 40-dB noise and when using BEM. Q5 refers to the potential distributions at 5 ms after the Q-onset; the same applies to Q10 and Q15; Qpk refers to the distributions at the peak of the Q-wave. See Table 1 for explanations of acronyms describing regularization methods.

	ZOT	FOT	SOT	ZCG	FCG	SCG	ZLSQR	FLSQR	SLSQR	TSVD	ν	FTV	STV	LASSO
Q_5	0.32	0.22	0.22	0.32	0.25	0.25	0.32	0.25	0.25	0.33	0.32	0.23	0.22	0.36
Q_{10}	0.26	0.11	0.10	0.26	0.11	0.11	0.26	0.11	0.11	0.27	0.26	0.15	0.12	0.26
Q_{15}	0.30	0.18	0.16	0.26	0.19	0.15	0.26	0.19	0.15	0.27	0.27	0.14	0.13	0.27
Q_{pk}	0.49	0.43	0.39	0.40	0.45	0.38	0.40	0.45	0.38	0.44	0.45	0.31	0.25	0.40

Table 3. Root-mean-square (rms) errors for reconstruction results for standard reference points of the sinus rhythm (peaks of P, R, S, and T waves) in the presence of a 40-db noise and when using BEM. See Table 1 for explanations of acronyms describing regularization methods.

	ZOT	FOT	SOT	ZCG	FCG	SCG	ZLSQR	FLSQR	SLSQR	TSVD	ν	FTV	STV	LASSO
P	0.47	0.43	0.42	0.47	0.45	0.45	0.47	0.45	0.45	0.51	0.48	0.37	0.41	0.45
R	0.45	0.40	0.39	0.40	0.40	0.38	0.40	0.40	0.38	0.42	0.43	0.35	0.33	0.40
S	0.48	0.42	0.40	0.47	0.45	0.44	0.47	0.45	0.44	0.50	0.49	0.37	0.40	0.45
T	0.27	0.16	0.16	0.26	0.16	0.16	0.26	0.16	0.16	0.27	0.26	0.17	0.16	0.26

was done for the isotropic and homogeneous volume conductor model, while FEM can incorporate more complex electric properties of the volume conductor than BEM.

Computational times of individual regularization techniques varied, with the iterative methods being far the fastest (on average 2 sec per one reconstruction). Due to the nature of Tikhonov and non-quadratic regularizations, which employ the penalty functions, we need to compute a large number (typically 20 to 40) of regularized solutions to determine the optimal one. As a consequence, it takes on average 8 sec per one reconstruction when using Tikhonov and 180 sec when using FTV and STV. Among, non-quadratic methods, LASSO requires least computational time (less than 2 sec per reconstruction).

4 Discussions

The main finding of our study is that non-quadratic methods (FTV and STV) have proven more robust to the complexity of the spatial patterns and noise in reconstructing the cylindrical-cage potentials. This conclusion is in agreement with the recent study of Gosh and Rudy [4], who noted that TV method (also called L1 regularization) may better capture spatial pattern of epicardial potentials than techniques, which minimize the square of the norm.

In our study, we compared the performance of various regularization techniques using a physiological model of the canine heart. This is the initial step of comprehensive validation and in our future work we will employ simultaneously measured body surface and epicardial potentials and experimental protocols, which will identify the sites of early activation both during pacing and in the models of infarcted hearts.

References

[1] H. S. Oster, B. Taccardi, R. L. Lux: P. R. Ershler, Y. Rudy: Noninvasive electrocardiographic imaging: Reconstruction of epicardial potentials, electrograms, isochrones and localization of single and multiple electrocardiac events. Circulation 1997, **96:** 1012-1024.

[2] Y. Rudy, B. J. Messinger-Rapport: The inverse problem in electrocardiography: Solutions in terms of epicardial potentials. CRC Crit. Rev. Biomed. Eng. 16: 215-268.

[3] R. Hren: Value of epicardial potential maps in localizing pre-excitation sites for radiofrequency ablation. A simulation study. Phys. Med. Biol. 1998, **43**:1449-1468.

[4] S. Ghosh, Y. Rudy: Application of L1-norm regularization to epicardial potential solution of the inverse electrocardiography problem. Ann. Biomed. Eng. 2009, 37: 902-912.

[5] B. M. Horacek, J. C. Clements: The inverse problem of electrocardiography: a solution in terms of single- and double-layer sources of the epicardial surface. Math Biosci 1997, 144: 119-154.

[6] A. Tikhonov, V. Arsenin: Solution of Ill-Posed Problems. Washington, DC: Winston, 1977.

[7] D. H. Brooks, F. A. Ghandi, R. S. MacLeod: Inverse electrocardiography by simultaneous imposition of multiple constraints, IEEE Trans. Biomed. Eng. 1999, **46**: 3-18.

[8] M. Hanke: Conjugate Gradient Type Methods for Ill-Posed Problems. Harlow: Longman Scientific & Technical, 1995.

[9] C. C. Paige, M. A. Saunders: LSQR: An algorithm for sparse linear equations and sparse least squares, ACM Transactions on Mathematical Software 1982, **8**: 43-71.

[10] P. C. Hansen: Rank-Deficient and Discrete Ill-Posed Problems. Philadelphia: SIAM, 1998.

[11] M. Schmidt: Least Squares Optimization with L1-Norm Regularization, Project Report , University of British Columbia, 2005